Article

Fast-forming hydrogel with ultralow polymeric content as an artificial vitreous body

Accepted Manuscript

Publication reference:
Hayashi, K., Okamoto, F., Hoshi, S. *et al.* Fast-forming hydrogel with ultralow polymeric content as an artificial vitreous body. *Nat Biomed Eng* **1**, 0044 (2017).

DOI of published article:
https://doi.org/10.1038/s41551-017-0044

Submitted to Nature Biomedical Engineering
submitted December 9, 2016
revised January 28, 2017

Article

Fast-forming hydrogel with ultralow polymeric content as an artificial vitreous body

Kaori Hayashi[1], Fumiki Okamoto (co-first author)*[2], Sujin Hoshi[2], Takuya Katashima[3], Denise Zujur[1], Xiang Li[4], Mitsuhiro Shibayama[4], Elliot P. Gilbert[5], Ung-il Chung[1], Shinsuke Ohba[1], Tetsuro Oshika[2], Takamasa Sakai*[1, 6]

1. Department of Bioengineering, Graduate School of Engineering, The University of Tokyo, 7-3-1 Hongo, Bunkyo-ku, Tokyo 113-8656, Japan

2. Department of Ophthalmology, Faculty of Medicine, University of Tsukuba, 1-1-1 Tennoudai, Tsukuba, Ibaraki, 305-8575 Japan

3. Department of Macromolecular Science, Graduate School of Science Osaka University 1-1 Machikaneyama-cho, Toyonaka, Osaka, 560-0043, Japan

4. Institute for Solid State Physics, The University of Tokyo, 5-1-5 Kashiwanoha, Kashiwa, Chiba, 277-8583, Japan

5. Australian Centre for Neutron Scattering, Australian Nuclear Science and Technology Organisation, Locked Bag 2001, Kirrawee DC, NSW 2232, Australia

6. PREST, JST

* *To whom correspondence should be addressed*.

Summary Paragraph

Degradation-induced swelling in implanted hydrogels can cause severe adverse reactions to surrounding tissues. Here, we report a new class of hydrogel with extremely low swelling pressure, and demonstrate its use as an artificial vitreous body. The hydrogel has ultralow polymer content (4.0 g/L), low cytotoxicity, and forms in situ in 10 minutes via the crosslinking of clusters of highly branched polymers of tetra-armed poly(ethylene glycol) pre-polymers. After injection and gelation in the eyes of rabbits, the hydrogel functioned as an artificial vitreous body for over a year without adverse effects, and proved effective for the treatment of retinal detachment. The properties of the cluster hydrogel make it a promising candidate as an infill biomaterial for a range of biomedical applications.

Main text

Biomedical Application of Injectable hydrogels

If a material can be introduced without a surgical procedure, treats the disease, and does not harm surrounding tissues throughout its full lifecycle *in vivo*, this represents a significant advance as a biomaterial. Such minimally invasive installation can be achieved using hydrogels by simply injecting a polymer solution into a target space, followed by crosslinking [1-4]. The solution eventually becomes a hydrogel (**Figure 1, top**) and fills the space inside the body. However, with regard to the final destination, conventional hydrogels have undesirable properties (i.e. swelling) that compromise their morphological and mechanical compatibility *in vivo*. Immediately after installation, such *in situ*-forming hydrogels have a higher osmotic pressure (Π_{os}) than the physiological aqueous environment. Due to the difference in osmotic pressure, the hydrogel absorbs water from the surrounding environment, resulting in swelling. The swelling induces an elastic pressure within the hydrogel (Π_{el}) that acts to oppose swelling. Since Π_{os} is much larger than Π_{el} in a good solvent, most hydrogels swell in aqueous conditions with a swelling pressure of Π_{sw}.

$$\Pi_{sw} = \Pi_{os} - \Pi_{el} \qquad (1)$$

These pressures get balanced after a certain magnitude of swelling, achieving an equilibrium

swollen state ($\Pi_{sw} = 0$) [5]. It is noteworthy that this equilibrium is transient since hydrogel degradation decreases Π_{el} and shifts the equilibrium to a more swollen condition, leading to extra swelling.[6, 7] Because conventional hydrogels degrade on a long-term basis in *vivo*, extra swelling may be delayed, but cannot be prevented, even in the case of "non-swellable" hydrogels [8]. Extra swelling has caused serious adverse reactions in ophthalmological applications. For example, Mira Gel® was commercialized in the 1980s as an eye buckle for the treatment of detached retinas [9, 10]; more than 7 years after installation, the degraded Mira Gel began to swell in the eye socket and eventually compressed the eyeball, resulting in blindness in some cases [11, 12]. Based on the equation (1), the maximum Π_{sw} that can be exerted by the hydrogel is Π_{os}. To completely eliminate the problems caused by swelling, it is important to reduce Π_{os} of hydrogels.

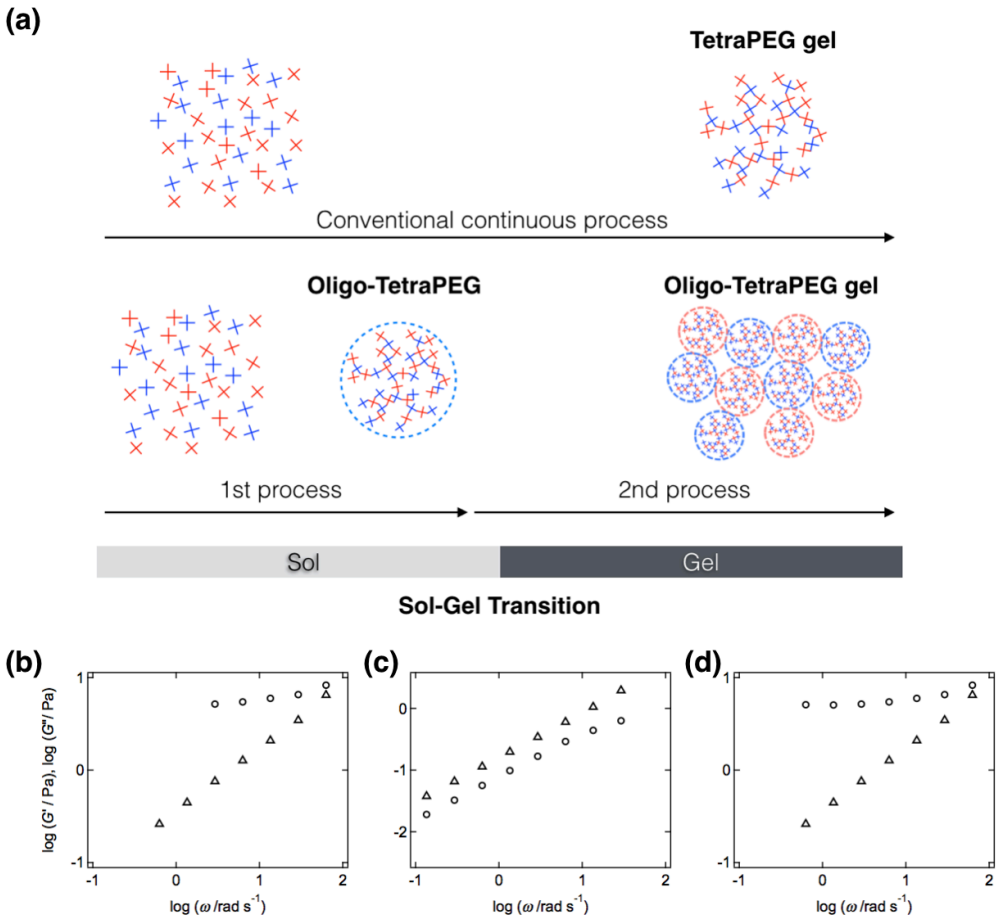

Figure 1. (a) Schematic illustration of gelation processes of conventional TetraPEG hydrogel and Oligo-TetraPEG hydrogel. In the conventional TetraPEG hydrogel system, mutually reactive TetraPEGs are simply mixed and reacted with each other to form the hydrogel. In the case of the Oligo-TetraPEG hydrogel system, first mutually reactive TetraPEGs were mixed in TetraPEG-SH excess and TetraPEG-MA excess conditions to form highly branched polymeric clusters instead of hydrogels (Oligo-TetraPEGs). In the second *vivo* process, mutually reactive Oligo-TetraPEGs were mixed to form Oligo-TetraPEG hydrogel. (b) (c) and (d) show the storage modulus, G', (circles) and loss modulus, G'', (triangles) as a function of frequency, ω, below, at and above the gelation threshold, respectively. In the region below the gelation threshold (b, $c_0 = 60$ g/L, $r = 0.15$), the system is in the sol state and $G' < G''$. At the gelation threshold (c, $c_0 = 60$ g/L, $r = r_c = 0.16$), the system transforms from a sol to a gel and shows a unique power law behaviour, $G' \approx G'' \approx \omega^{\beta}$. Above the gelation threshold (d, $c_0 = 60$ g/L, $r = 0.17$), the system is in the gel state and $G' > G''$ in a wide range of ω. All the experiments were performed in triplicate and the data were averaged for each ω. The lengths of error bars (S.D.) are smaller than the size of symbols.

One of the simplest methodologies for reducing Π_{os} is to decrease the polymer concentration [13,14]; however, the inherent, critical problem of this approach is the challenge of gel formation. Even in an ideal model gel system (Tetra-PEG (TP) gel) [15,16], the lowest gelation polymer concentration is 6.0 g/L with 7 hours being required for gelation (**Figure 2a**), the latter far exceeding the time scale of surgery. To prepare an *in situ*-forming hydrogel with a lower polymeric content, and, in addition, that can efficiently form a three-dimensional (3D) polymer network within a reasonable time frame, the design and fabrication of a brand new class of polymeric modules is essential. Here, we describe an *in situ*-forming hydrogel system that can be formed using an extremely low polymer content (~ 4.0 g/L) within 10 minutes. We demonstrate the application of the hydrogel as an artificial vitreous body for treating retinal detachment.

Design of Fast-forming Hydrogels with Low-Polymer Content

At the beginning of conventional crosslinking reaction of polymers (**Figure 1a, top**), the system is still a solution, where the loss modulus (G'') is larger than the storage modulus (G') in the whole frequency region (**Figure 1b**). Here, G'' and G' are indicators of the liquid-like and

104 solid-like nature of the material, respectively. During the gelation, the polymer chains are
105 connected to each other to form a highly branched polymeric structure (polymeric clusters).
106 The polymeric clusters further grow and eventually form a 3D polymer network percolating
107 through space at the gelation point. At the gelation point, the system transforms from a sol to
108 a gel, and shows a unique power law behaviour, i.e., $G' \approx G'' \sim \omega^{\beta}$ (**Figure 1c** and
109 **Supplementary Figure 1**) [17,18]. Above the gelation point, the system becomes a gel, which
110 has no fluidity, and G' becomes larger than G'' over a wide range of ω (**Figure 1d**). In our
111 novel system, we separate the challenge of gelation at low polymer content into two processes
112 (**Figure 1a, bottom**). In the first process, the reaction is intentionally stopped immediately
113 prior to the gelation point (**Figure 2a**), at which stage polymeric clusters nearly percolate
114 through the system. The resulting Oligo-TetraPEG exhibits a unimodal size distribution of up
115 to 90 nm (**Supplementary Figure 2**), which is much larger than those of conventional hyper-
116 branch polymers[19,20], suggesting that the Oligo-TetraPEG has a highly branched structure. In
117 the second process, the Oligo-TetraPEGs are co-crosslinked as individual modules to
118 expeditiously form a hydrogel (Oligo-TetraPEG (Oligo-TP) hydrogels).
119

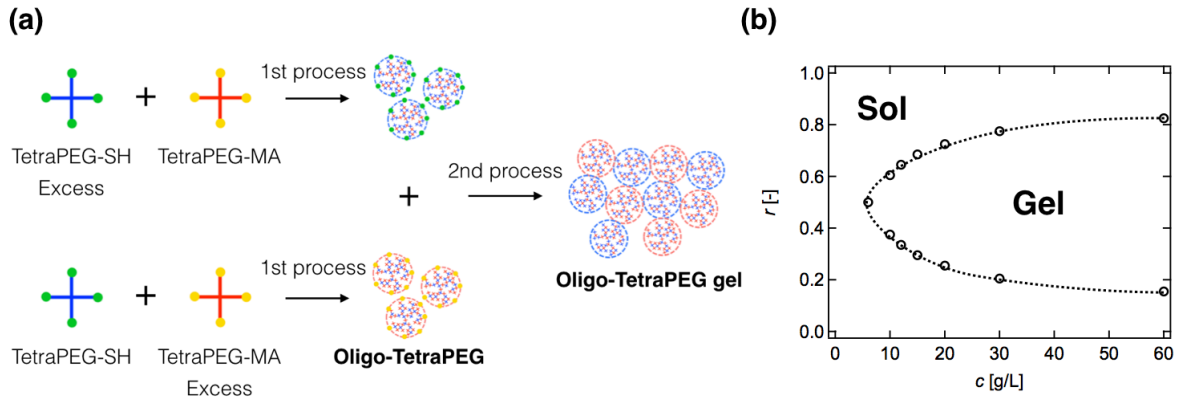

Figure 2. (a) Fabrication process for Oligo-TetraPEG hydrogel through the two step process. In the first process, TetraPEG-SH and TetraPEG-MA were mixed in non-stoichiometric conditions to form SH-excess and MA-excess Oligo-TetraPEGs. In the second process, these Oligo-TetraPEG solutions were equally diluted and mixed in equal amount to form Oligo-TetraPEG hydrogels. (b) Sol-gel phase diagram: the relationship between initial polymer concentration (c_0) and mixing ratio of TetraPEG-SH to total polymer concentration (r = [TetraPEG-SH]/([TetraPEG-SH] + [TetraPEG-MA])) at sol-gel transition points. The conditions inside the dotted line produced gels, while the conditions outside did not. All the experiments were performed in triplicate and averaged. The lengths of error bars (S.D.) are smaller than the size of symbols.

Fabrication and Characterization of Oligo-TetraPEG hydrogels

To systematically form Oligo-TetraPEGs, we utilized mutually reactive tetra-armed prepolymers including tetra-armed polyethyleneglycol (PEG) with thiol termini (TetraPEG-SH) and maleimide termini (TetraPEG-MA) (**Figure 2a**) [21]. First, we investigated the critical ratio forming hydrogels (r_c) by tuning the molar ratio of these prepolymers (r = [TetraPEG-SH] / ([TetraPEG-SH] + [TetraPEG-MA])) for each initial polymer concentration (c_0). As shown in **Figure 2b**, the stoichiometric conditions (r_c = 0.5) produced hydrogels in the region $c_0 > 6.0$

g/L, and the r region that produced hydrogels decreased with a decrease in c_0. The Oligo-TetraPEGs are, thus, formed in the sol region close to the sol-gel transition line. In the case of 60 g/L, MA-excess and SH-excess Oligo-TetraPEGs were formed at r = 0.13 and 0.87, respectively (r_c = 0.16 and 0.83). Based on UV spectroscopy, nearly all minor species reacted with excess species (**Supplementary Figure 3**), indicating that only the excess functional group exists on each Oligo-TetraPEGs.

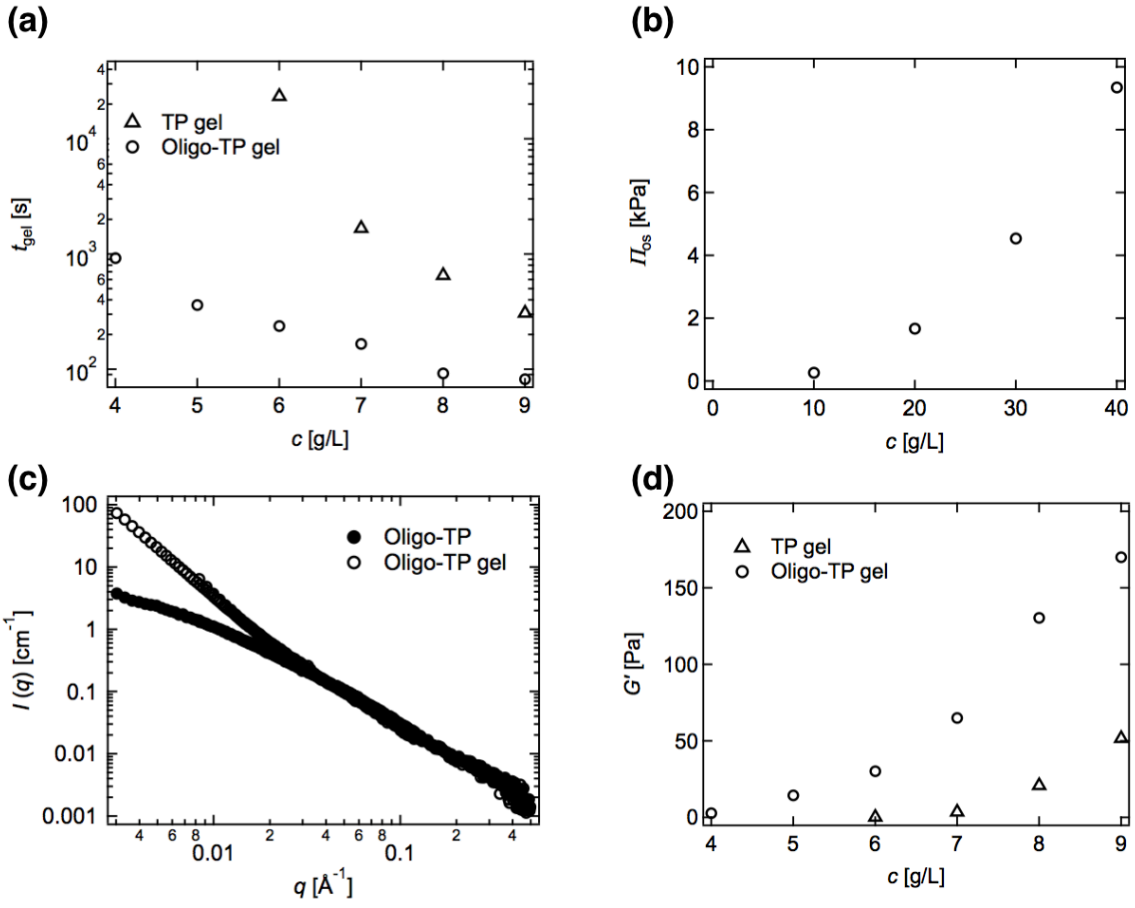

Figure 3. (a) Gelation time (t_{gel}) of Oligo-TP hydrogels (circles) and TP hydrogels (triangles) as a function of the polymer concentration (c). (b) Osmotic pressure (Π_{os}) of Oligo-TP hydrogels as a function of c. (c) SANS measurements from an Oligo-TP solution and an Oligo-TP hydrogel. (d) Equilibrium storage modulus (G') of Oligo-TP hydrogels (circles) and TP hydrogels (triangles) as a function of c. All the experiments except for

SANS measurements were performed in triplicate and averaged. The lengths of error bars (S.D.) are smaller than the size of symbols. The error bars on the SANS profiles show S.D following complete data processing.

In the second process, we co-crosslinked the mutually reactive Oligo-TetraPEGs (MA-excess and SH-excess Oligo-TetraPEGs) to form Oligo-TetraPEG hydrogels (**Figure 2a**). Each Oligo-TetraPEG solution was diluted to the same specific concentration (c) and mixed with each other in equal amount. **Figure 3a** shows the gelation time (t_{gel}) as a function of c. For direct comparison, the results from the conventional one-step method in which hydrogels were directly prepared using the first process with r = 0.5, i.e. TetraPEG hydrogels, are also presented. In the case of Oligo-TetraPEG hydrogels, t_{gel} decreased significantly and to nearly within the desired range, i.e. less than 10 minutes. In addition to the shortened t_{gel}, the lowest concentration for gelation and consequently hydrogel formation decreased to c = 4.0 g/L; this is lower than that of the hydrogel with the lowest network concentration [22]. It should be noted that it is difficult to accelerate gelation reactions properly by tuning the reactivity of functional groups; too great a level of active species may result in sudden and heterogeneous gelation, because gelation occurs prior to the homogeneous mixing of prepolymers. In our methodology, we can continuously and easily control the 'distance' to the gel point by tuning r in the first process forming Oligo-TetraPEGs, resulting in the appropriate approach to gelation. Π_{os} of Oligo-TetraPEG hydrogels was a positive finite value and lower than typical eye pressure

(~1 kPa) in the region c < 10 g/L (**Figure 3b**). Based on small-angle neutron scattering (SANS) measurements, the Oligo-TetraPEG hydrogel has a similar structure to the Oligo-TetraPEG in the high-q region (0.03 $Å^{-1}$ < q) together with a highly heterogeneous structure with a wide and smooth size distribution in the low-q region (q < 0.03 $Å^{-1}$) (**Figure 3c**), where q is the magnitude of the scattering vector (a measure of a reciprocal length scale). The typical size of the heterogeneity is smaller than the wavelength of visible light, because the Oligo-TetraPEG hydrogel was transparent. The plateau moduli (G') of Oligo-TetraPEG hydrogels were always higher than those of the conventional hydrogels with the same c (**Figure 3d**), strongly suggest the efficient network formation. The obtained G' values cover the range of those of soft tissues, such as the vocal cord (10^2 - 10^3 Pa), vitreous body (10^0 - 10^1 Pa) and crystalline lens (10^2 - 10^3 Pa) (**Supplementary Movie 1**).

Biocompatibility of Oligo-TetraPEG hydrogels

We next evaluated biocompatibility of Oligo-TetraPEG hydrogel (c = 7.0 g/L, $G \approx$ 4 Pa) *in vivo* by subcutaneous injection into mice. After 4 weeks, Oligo-TetraPEG hydrogels still remained in the injected site without damage to adjacent tissues (**Figure 4a**). Histological analysis displayed mild infiltration of inflammatory cells in all tested materials. However, expression

of CD62L, a marker for inflammatory cells, and encapsulation of the material was detected only in the hydrogel formed from Oligo-TetraPEG crosslinked by small molecules (**Figure 4a**). Due to the similarity between gelation and reverse gelation (disintegration), Oligo-TetraPEGs are not only the raw materials but also the metabolites of Oligo-TetraPEG hydrogels. We thus examined the toxicity of the Oligo-TetraPEGs, and confirmed low toxicities of these specimens *in vitro* (**Figure 4b**) and *in vivo* (**Figure 4c and Supplementary Figure 4**). The low toxicity of Oligo-TetraPEGs may stem from the low permeability of extremely large Oligo-TetraPEGs through the pores of surrounding tissues. These results strongly suggest the biosafety of the full lifecycle of Oligo-TetraPEG hydrogels from formation to disintegration.

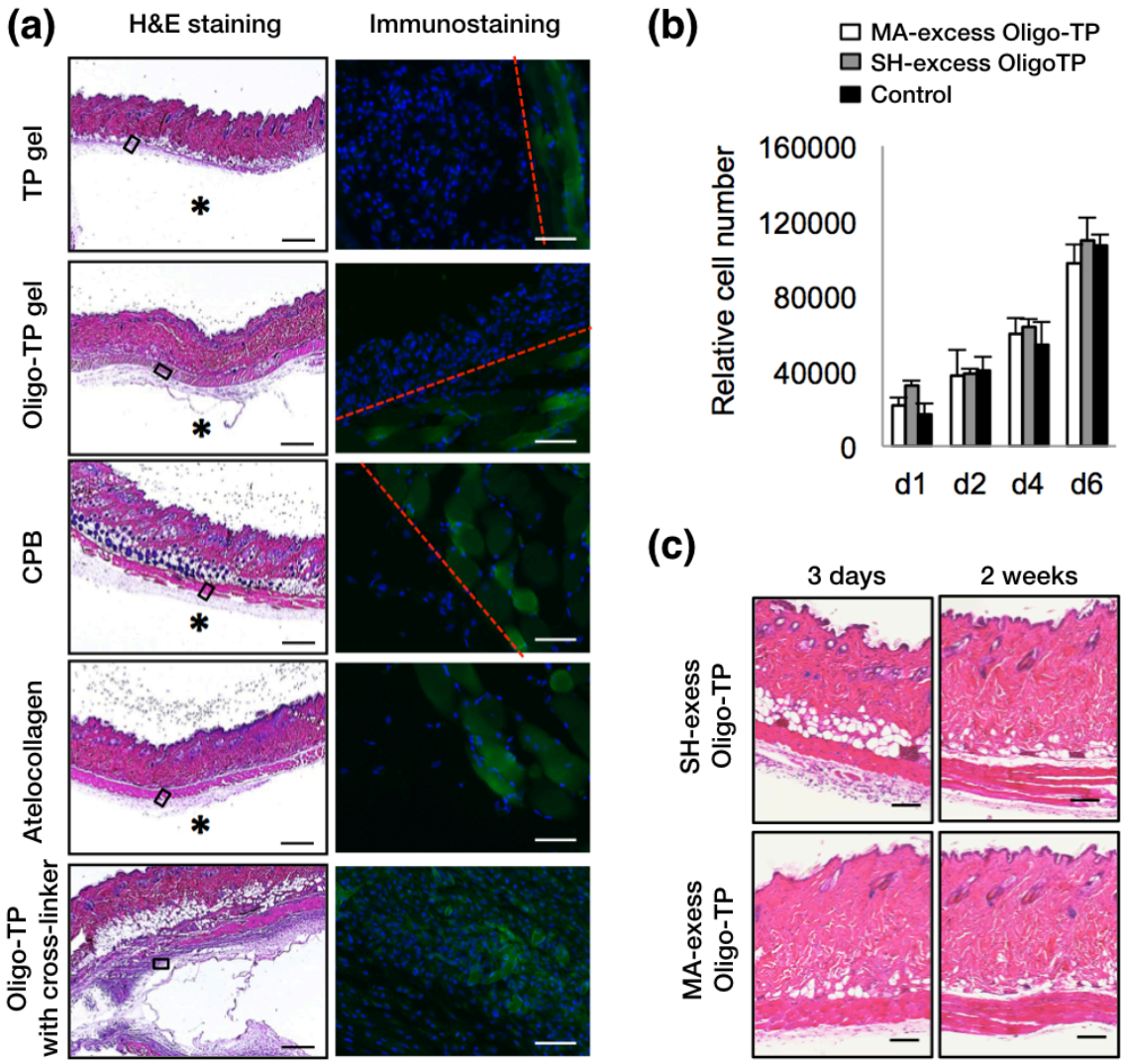

198

199 **Figure 4. (a) Gel specimens and surrounding tissues, representative images of H&E**
200 **staining and immunostaining for CD62L (GFP) in histological sections of mice at 4 weeks**
201 **after subcutaneous injection of materials. Asterisks, arrows and rectangles denote**
202 **materials, epidermis and the location of views of immunostaining, respectively. Nuclei**
203 **were stained with DAPI. Non-specific GFP signal was detected in muscles (red dotted**
204 **lines). Scale bars in H&E staining and immunostaining indicate 5 mm and 100 μm,**
205 **respectively. (b) Cell proliferation of NIH3T3 cells cultured with or without Oligo-**
206 **TetraPEGs. The data (relative cell number) are expressed as the mean ± SDs from four**
207 **independent experiments. No statistical difference was found between MA-excess Oligo-**
208 **TP and control, SH-excess Oligo-TP and control, and MA excess and SH excess Oligo-TPs**
209 **in Student t-test analysis. (c) Representative H&E staining images of histological sections**
210 **in mice subcutaneously injected with MA-excess and SH-excess Oligo-TPs or PBS.**
211 **Sections at 3 days and 2 weeks after the injection are shown. Scale bars, 200 *μ*m.**

212

213 ***Applicability to Artificial Vitreous Body***

214 The low cytotoxicity and extremely low swelling pressure of Oligo-TetraPEG hydrogels led us
215 to examine the possibility of its application as an artificial vitreous body. Although a variety
216 of artificial vitreous bodies have been developed, most of them induce an ocular inflammatory
217 reaction in animal studies, preventing clinical application in humans [23-27]. The
218 biocompatibility and effectiveness of Oligo-TetraPEG hydrogels (c = 7.0 g/L, $G \approx 4$ Pa) were
219 evaluated using the normal Dutch pigmented rabbit model (**Supplementary Movie 2**) [28]. The
220 Oligo-TetraPEG pre-gel solution was compatible with the modality of current small-gauge
221 incision vitreous surgeries and subsequently formed a hydrogel within the vitreous cavity. No
222 significant difference in intraocular pressure was observed between Oligo-TetraPEG hydrogel-
223 injected and balanced salt solution-injected (control) groups throughout the observation period,
224 up to 410 days (**Figure 5a**). Based on slit lamp examinations (**Figure 5b**), images of eyes
225 after dissection (**Figure 5c**), and H&E staining in histological section (**Figure 5g**), neither
226 significant inflammation nor toxic reaction was observed. Remaining Oligo-TetraPEG
227 hydrogel in the vitreous cavity was detected by slit lamp biomicroscopy with a 90-D fundus
228 lens; however it was not detected with histological analysis probably because of technical

229 limitations during histological sectioning. Electroretinography to assess retinal function
230 showed no significant difference in positive waveforms, implicit times and amplitudes between
231 Oligo-TetraPEG hydrogel-injected and control groups. (**Figure 5d, e, f**). Fundus photography
232 revealed that Oligo-TetraPEG hydrogel remained transparent throughout the follow-up period
233 inside the vitreous cavity of the living rabbit eyes (**Figure 6**). Spectral-domain optical
234 coherence tomography revealed neither retinal detachment nor oedema, and the retinal
235 microstructure was not morphologically damaged in either group. By contrast, lens opacity
236 (**Figure 5b**), vitreous opacity (**Figure 5c**) and negative waveforms of electroretinography
237 (**Figure 5d**) due to severe inflammation were observed in the high polymer concentration group
238 (c = 60 g/L, $G \approx$ 9.5 kPa), similar to the previous artificial vitreous materials. The turbidity in
239 the eyes prevented images of the retina from being obtained through the vitreous. Intraocular
240 pressure could not be measured correctly because of postoperative inflammatory corneal
241 melting in this group as well. In addition, we developed an animal model of retinal
242 detachment and injected Oligo-TetraPEG hydrogel into the vitreous cavity as a vitreous
243 tamponade material to evaluate if pathological conditions could be treated with the gel. As a
244 result, retinal re-detachment was inhibited for 410 days without any complications (**Figure 6**).

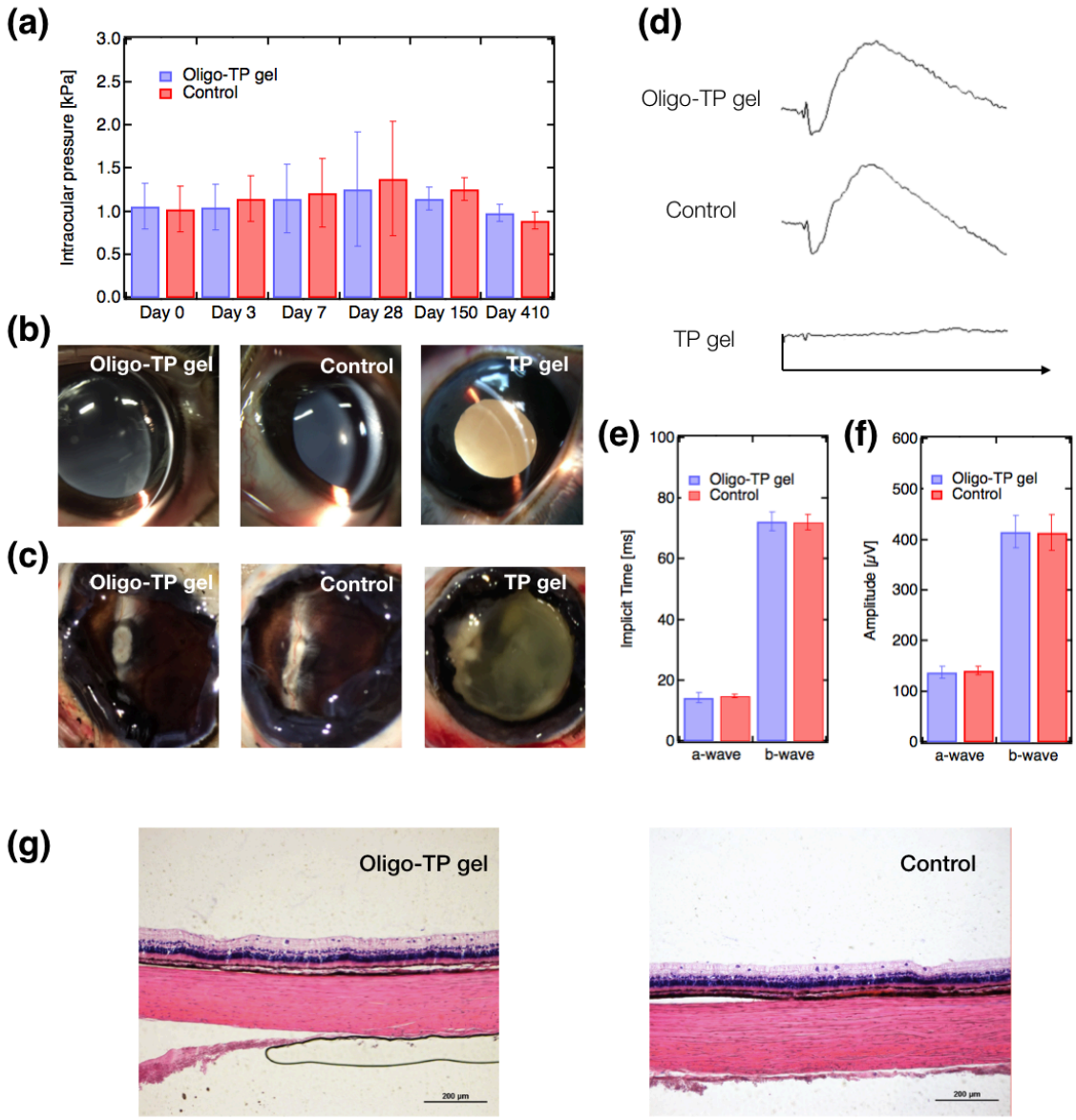

Figure 5. (a) Changes in the intraocular pressure in the Oligo-TP hydrogel-injected and balanced salt solution-injected (control) groups. No significant difference in intraocular pressure was observed between Oligo-TP hydrogel-injected and control groups throughout the observation period, up to 410 days in Student t-test analysis. The data are expressed as the mean ± SDs. (b) Anterior segments of rabbit eyes in the Oligo-TP hydrogel-injected, control and TP hydrogel-injected groups on postoperative day 7. (c) Images of eyes after dissection 90 days postoperatively in the Oligo-TP hydrogel-injected, control and TP hydrogel-injected groups. (d) Electroretinography waveform of rabbit eyes in the Oligo-TP hydrogel-injected, control and TP hydrogel-injected groups on postoperative day 90. Bars: 100 μV and 25 ms. (e) Electroretinography data of a-wave and b-wave implicit time in the Oligo-TP hydrogel-injected and control groups on postoperative day 90. The data are expressed as the mean ± SDs. (f) Electroretinography

data of a-wave and b-wave amplitudes in the Oligo-TP hydrogel-injected and control groups on postoperative day 90. The data are expressed as the mean ± SDs. No significant difference in implicit times and amplitudes was observed between Oligo-TP hydrogel-injected and control groups. (g) Representative images of H&E staining in histological section of rabbit eyes at 410 days postoperatively. Scale bars indicate 200 μm. No apparent inflammation or alteration of retinal microstructure was observed in both Oligo-TP hydrogel-injected and control group.

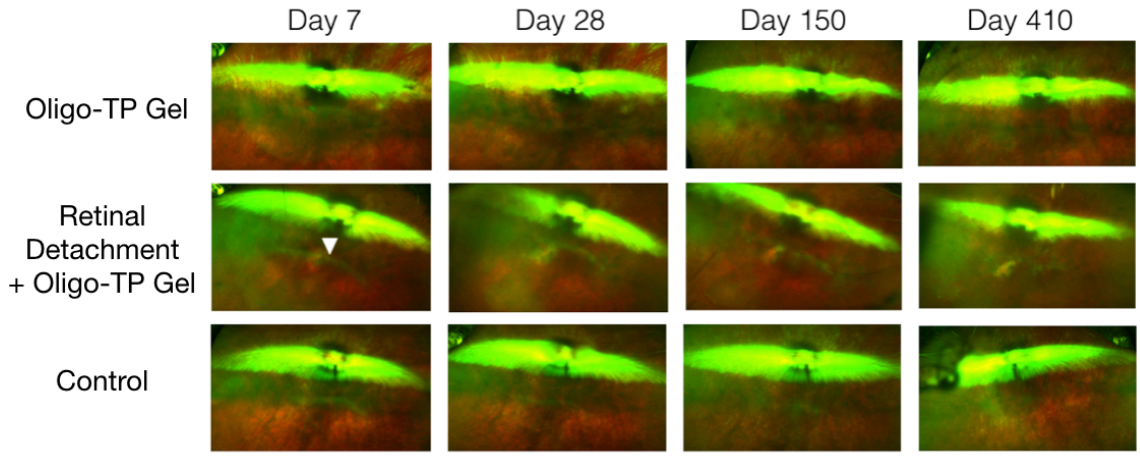

Figure 6. Fundus photography of rabbit eyes in the Oligo-TP hydrogel-injected, retinal detachment with the Oligo-TP hydrogel-injected and control groups. Arrowhead = intentional retinal break.

Discussion

The Oligo-TetraPEG hydrogel was non-invasively installed within a clinically relevant manipulation time and provided low potential swelling pressure throughout the full life cycle *in vivo*. We have further provided a proof of concept for the application of the gel as an artificial vitreous body. Given that their elastic moduli cover the range of those of soft tissues,

Oligo-TetraPEG hydrogels will maximize their ability when used as a space-filling implant in unloaded soft tissues, e.g., craniofacial soft tissues; they can be potentially applied to the filling of postsurgical cavities accompanied with re-section of soft tissues that are damaged by trauma, tumor, inflammation, degeneration, and so on, as well as tissue augmentation for cosmetic purposes and the prevention of postoperative adhesions. When complemented by additional functions, such as drug carriers and/or disease modifiers as well as space fillers, these gels could treat a broader range of trauma and degenerative diseases. The repair of sensory and locomotive organs could exploit full life cycle safety because joints, eyes, and ears form confined spaces that house their components and function. Since trauma and degenerative diseases of these organs threaten the quality of life (QOL) of elderly patients, this Oligo-TetraPEG hydrogel may help resolve the gap between life expectancy and healthy life expectancy confronting our progressively ageing society.

Acknowledgements

This work was supported by the Japan Society for the Promotion of Science (JSPS) through Grants-in-Aid for the Graduate Program for Leaders in Life Innovation (GPLLI), the International Core Research Center for Nanobio, Core-to-Core Program A. Advanced Research Networks, and Grants-in-Aid for Young Scientists (A) Grant Number 23700555 to TS, Scientific Research (S) Grant Number 16H06312 to UC, and Scientific Research (C) Grant Number 26462631 to FO. This work was also supported by the Japan Science and Technology Agency (JST) through the S-innovation program and Center of Innovation program (to UC) and PREST (to TS).

Methods

1. Sol-gel transition diagram

TetraPEG-SH and tetraPEG-MA were purchased from NOF Co. (Tokyo, Japan). The molecular weights of Tetra-PEG-SH and Tetra PEG-MA were 10 kg/mol. TetraPEG-SH and tetraPEG-MA were dissolved in citric-phosphate acid buffer (CPB) (pH5.0, salt concentration: 5.0 mM); c_0 = 60 g/L, r = 0.13, 0.14, 0.15, 0.16, 0.17, 0.81, 0.82, 0.83, 0.84 and 0.85; c_0 = 30 g/L, r = 0.18, 0.19, 0.20, 0.21, 0.22, 0.76, 0.77, 0.78, 0.79 and 0.80; c_0 = 20 g/L, r = 0.23, 0.24, 0.25, 0.26, 0.27, 0.71, 0.72, 0.73, 0.74 and 0.75; c_0 = 15 g/L, r = 0.27, 0.28, 0.29, 0.30, 0.31, 0.67, 0.68, 0.69, 0.70 and 0.71; c_0 = 12 g/L, r = 0.31, 0.32, 0.33, 0.34, 0.35, 0.63, 0.64, 0.65,

0.66 and 0.67; c_0 = 10 g/L, r = 0.35, 0.36, 0.37, 0.38, 0.39, 0.59, 0.60, 0.61, 0.62 and 0.63. The same amount of the resultant solutions were mixed while tuning the total polymer concentrations (c_0) and the off-stoichiometry ratios of tetra-PEG-SH (r). The resulting solutions were poured into the gap within the double cylinder of a rheometer. The oscillatory shear rheological properties (the storage elastic modulus (G') and the loss elastic modulus (G")) during gelation were measured at 25℃ with double cylinder geometry (MCR301; Anton Paar, Switzerland). The applied strain and the frequency were 1.0% and 1.0 Hz, respectively. After 12 hours, the frequency-dependence of G' and G" were measured at a constant strain (1.0%) and frequency of 0.1 - 100 rad/sec. The critical molar ratios were determined as per the criteria of Winter and Chambon [17,18].

2. Fabrication of Oligo-TetraPEG hydrogel

An appropriate quantity of TetraPEG-SH and TetraPEG-MA were separately dissolved in citric-phosphate acid buffer (CPB) (pH5.0, salt concentration: 5.0 mM). Equal amounts of TetraPEG-SH (7.4 g/L) and TetraPEG-MA (12.6 g/L) solutions were subsequently mixed. In another vial, an equal amount of TetraPEG-SH (12.6 g/L) and TetraPEG-MA (7.4 g/L) solutions were mixed. The two solutions were left to stand at least for 12 h. The two resultant solutions were diluted by using CPB into c = 4.0, 5.0, 6.0, 7.0, 8.0 and 9.0 g/L. Equal amounts of equally diluted solutions were mixed; each resulting solution was left to stand at least for 12 h.

3. Fabrication of conventional Tetra-PEG gel

TetraPEG-SH (4.0, 5.0, 6.0, 7.0, 8.0 and 9.0 g/L) and TetraPEG-MA (4.0, 5.0, 6.0, 7.0, 8.0 and

9.0 g/L) were dissolved in citric-phosphate acid buffer (CPB) (pH5.0, salt concentration: 5.0 mM). Two TetraPEG-SH and TetraPEG-MA solutions with the same concentration were mixed in equal amounts. The resulting solutions were left to stand at least for 12 h.

4. Dynamic Light scattering

DLS measurements were performed on an ALV/CGS-3 goniometer system (ALV, Germany). A He-Ne laser with a power of 22 mW emitting polarized light at 632.8 nm was used. Correlation functions at scattering angle 90° were taken at 25℃. Each resultant solution was diluted to 1.0 g/L. The measurement time was 30 sec with 100 measurements for each sample.

5. UV spectra measurement

The reaction conversions of the minor species to excess species were estimated by ultraviolet and visible absorption spectroscopy (V-670; JASCO, Japan). TetraPEG-MA has a specific absorption peak arising from the maleimide group around 300 nm. This peak decreases with the reaction of tetraPEG-MA and tetraPEG-SH. Resultant solutions were poured into the cell (wavelength range: 285-750 nm, optical path length: 5 mm), and the absorbance was measured at a wavelength of 310nm. Here, the concentration of tetraPEG-MA was adjusted so that the absorbance at 310 nm was less than 1.0. Reaction conversion of the minor species to excess species in the solution were calculated by using absorbance at wavelength 310 nm and initial absorbance of tetra-PEG-MA, which was obtained by the calibration curve of tetraPEG-MA at wavelength 310 nm.

6. Swelling pressure measurement

Oligo-TetraPEG hydrogels were formed in dialysis membrane with molecular weight cut-off of 1.0k Da. The total weights of specimens and membranes were measured. The hydrogels packed in membranes were immersed into the aqueous solutions of polyvinylpyrrolidone (PVP) with molecular weight of 20k Da. The concentration of PVP solution was tuned from 10 to 120 g/L. After 2 days immersion at 25 ˚C, the weights of specimens were measured. Based on the difference in weight before and after the immersion, the concentrations of PVP that can suppress the swelling of hydrogel specimens (C_{PVP}) were measured. The swelling pressures of hydrogels (Π_{sw}) were calculated by the following equation.[29, 30]

$$\Pi_{\mathrm{sw}} = 0.878C_{\mathrm{PVP}} + 17.25{C_{\mathrm{PVP}}}^2 + 144.1{C_{\mathrm{PVP}}}^3$$

7. Small-angle neutron scattering

SANS experiments were performed on the QUOKKA instrument at the OPAL reactor at Australian Nuclear Science and Technology Organization (ANSTO), Sydney, Australia. Three configurations were used to yield a q range from 0.003 to 0.5 $Å^{-1}$, namely source-to-sample distances of 20m, 8m and 10m, and sample-to-detector distances of 20 m, 8 m and 1.3 m with 300 mm detector offset respectively. The wavelength of neutron beam was 5.0 Å with 10% wavelength resolution, with source and sample aperture diameters of 50 mm and 12.5 mm, respectively. All measurements were carried out at 25ºC. The Oligo-TetraPEG and Oligo-TetraPEG gel were prepared in D_2O buffer following the procedure of "2. Fabrication of Oligo-TetraPEG hydrogel".

8. Histological evaluation and immunostaining

For the biocompatibility study, some gel specimens*, Oligo-TetraPEGs or citric-phosphate acid

buffer (CPB) (pH5.0, salt concentration: 5.0 mM) with NaCl (salt concentration: 149 mM) (200 μl) were subcutaneously injected into the back of 5-week-old Crl:CD1 (ICR) male mice using a 26G needle. Given the Reduction in the 3Rs of animal welfare, we considered the sample size of three was appropriate to confirm the reproducibility of the histological findings in the pilot experiments with no quantitative analysis. Mice were randomly assigned to each group, and we were not blinded to the group allocation and the assessment of results. At 3 days, 2 weeks or 4 weeks following the injection, mice were sacrificed and the hydrogels and surrounding tissue were harvested. Collected samples were fixed in 4% paraformaldehyde and embedded in paraffin or OCT compound. Hematoxylin and eosin (H & E) staining was performed on de-paraffinized sections (5-7 μm). For immunostaining, cryosections (10 μm) were blocked with PBS containing 0.1% Triton X-100, 3% BSA (Sigma, A7906) and 1% heat inactivated sheep serum (Sigma, S2263) for an hour at room temperature. Sections were then incubated overnight at 4°C with anti-CD62L antibody (Abcam, ab119834; 1:200) and detection was achieved by subsequent incubation with Alexa Fluor® 488 (Abcam, ab172332; 1:500) for an hour at room temperature. Cell nuclei were stained with VECTASHIELD Mounting Medium containing DAPI (Vector Laboratories, H-1200). All experiments were performed in accord with the protocol approved by the Animal Care and Use Committee of The University of Tokyo (#KA14-3).

***Oligo-TetraPEG crosslinked hydrogels:**

Dithiol cross-linker (DL-(Dithiothreitol) (DTT)) was purchased from Sigma-Aldrich Japan (Tokyo, Japan). Oligo-TetraPEGs were fabricated with c_0 = 60 g/L and r_c = 0.13 in CPB (pH5.8, salt concentration: 5.0 mM) with NaCl (salt concentration: 149 mM). DTT was used as a cross-linker for Oligo-TetraPEGs. DTT was dissolved in CPB with NaCl with the equivalent

399 ratios to the number of unreacted functional groups in the Oligo-TetraPEG and mixed with
400 Oligo-TetraPEG solution, resulting in a solution with c = 13.5 g/L.
401 ***Oligo-TetraPEG hydrogel:**
402 Oligo-TetraPEGs were fabricated with c_0 = 60 g/L and r_c = 0.13, 0.87 in CPB (pH5.8, salt
403 concentration: 5.0 mM) with NaCl (salt concentration: 149 mM). These Oligo-TetraPEG
404 solutions were diluted to c = 7.0 g/L by using CPB with NaCl and mixed in equal amount.
405 ***Tetra-PEG gel:**
406 TetraPEG-SH and tetraPEG-MA were dissolved in CPB (pH5.8, salt concentration: 5.0 mM)
407 with NaCl (salt concentration: 149 mM) respectively. These two solutions were mixed to
408 produce a resultant solution with c = 15 g/L.
409 ***Atelocollagen gel:**
410 Atelocollagen gel (0.4 wt%) was produced from a commercially available bovine dermis
411 atelocollagen (Koken, KOU-IPC-50) following the manufacturer's instructions. Briefly, the gel
412 was obtained by mixing the acidic atelocollagen solution (5 mg/ml) with PBS, $NaHCO_3$,
413 HEPES (pH 7.4) and distilled water in an ice water bath.
414
415 **9. Cell proliferation assay**
416 NIH3T3 cells were obtained from RIKEN Cell Bank and cultured in the following media: basal
417 medium (BM) as a control (DMEM + 10% FBS + 1% pen-strep), BM + MA-excess Oligo-
418 TetraPEG, and BM + SH-excess Oligo-TetraPEG. NIH3T3 cells were periodically
419 authenticated by morphological inspection. We had confirmed no mycoplasma contamination
420 in the cell by a PCR-based mycoplasma detection assay (Venor GeM; Mineva Biolabs, Berlin,
421 Germany). The final concentration of the Oligo-TetraPEG in each medium was 20 mg/L. 5000

cells per well (100 μL) were inoculated in 96-well plates and pre-cultured in BM at 37 ˚C with 5% CO_2 for 24 hours. The medium was then replaced with the experimental ones and changed daily. Cell numbers from 4 independent wells per condition were counted on days 1, 2, 4 and 6 using Countess™ Automated Cell Counter (Invitrogen, C10227).

10. Animal model for vitreous body

Fourteen normal male Dutch pigmented rabbits, each weighing 2.0 to 3.0 kg, aged 2 to 3 months, were used. The study conformed to the ARVO Statement for the Use of Animals in Ophthalmic and Vision Research, and was reviewed and approved by the Animal Care and Use Committee of University of Tsukuba (#12-109). All procedures were carried out in left eyes with sterile techniques under a surgical microscope (Carl Zeiss Meditec, Inc., Oberkochen, Germany). The animals were anesthetized with intramuscular injection of ketamine hydrochloride (35 mg/kg) and xylazine (5 mg/kg). Topical anesthesia (0.4% oxybuprocaine hydrochloride drops) was applied to the eyes. Pupils were dilated with topical 0.5% phenylephrine hydrochloride, 0.5% tropicamide, and 1% atropine. A standard three-port, 25-gauge trocar-cannula vitrectomy system was used (Alcon Laboratories, Fort Worth, TX). An infusion cannula that delivered a balanced salt solution (BSS; Alcon Japan) was then inserted into the trocar cannula in the 2 o'clock position 1mm posterior to the limbus. The remaining two ports required for the insertion of a vitreous cutter and a light pipe in the 11 and 1 o'clock position, respectively, were created using the same method. The vitreous was detached from the retina by aspirating the cortical vitreous visualized with triamcinolone acetonide (Kenacort-A; Bristol-MyersSquibb, Tokyo, Japan). After removal of the vitreous with a vitrectomy cutter, air-fluid exchange was performed in the vitreous cavity. Following air–fluid exchange, 6 eyes of the rabbits were injected Oligo-

TetraPEG hydrogel* into the vitreous cavity, and 4 eyes of the rabbits were injected the conventional hydrogel*. A balanced salt solution was injected into the vitreous cavity of the remaining 4 rabbits as controls. Animals were randomized into the groups using envelopes. Sample sizes were based on pilot experiments. All scleral ports were closed with 8-0 Vicryl® after the injection of endotamponade.

11. Animal model for retinal detachment

Experimental retinal detachment with a break was made during a 25-gauge vitrectomy in 5 normal Dutch pigmented rabbit eyes. After removing the vitreous body, an extrusion needle was used to make a retinal break that was approximately 1/2-1 of the optic disc diameter (DD) in size. The break was made 2 DD inferior to the optic disc. An infusion stream of balanced salt solution was directed under the retinal break, which resulted in a localized retinal detachment of approximately 3-4 DD in size. To achieve retinal reattachment temporarily, air–fluid exchange through the retinal break was performed. After air-fluid exchange, Oligo-TetraPEG hydrogel* was injected into the vitreous cavity of 3 rabbits. A balanced salt solution was injected into the vitreous cavity of the remaining 2 rabbits as controls. Animals were randomized into the groups using envelopes. Sample sizes were based on pilot experiments. All scleral ports were closed with 8-0 Vicryl® after the injection of endotamponade.

* **Oligo-TetraPEG hydrogel:**

The Oligo-TetraPEG were fabricated with c_0 = 10 g/L and r = 0.32, 0.68 in CPB (pH5.8, 5.0 mM) with NaCl (149 mM). These two Oligo-TetraPEG solutions were diluted to c = 7.0 g/L by using CPB with NaCl and mixed in equal amount. The resultant solutions were mixed using the double syringe with three-way cock.

***Conventional hydrogel:**

TetraPEG-NH_2 and TetraPEG-NHS (60 g/L) were dissolved in PB (pH7.4, 50 mM) with NaCl (149 mM); the resultant solutions were mixed using the double syringe with three-way cock.

12. Intraocular pressure

The intraocular pressure was measured with a tonometer (icare pro; TA01i, Tiolat Oy, Finland) the day before surgery and 3, 7, 28, 90, 150 and 410 days after surgery. Measurements were conducted in a blinded manner.

13. Ocular examination

Slit lamp microscopy and indirect ophthalmoscopy were performed with dilated pupils under general anesthesia the day before surgery and 3, 7, 28, 90, 150 and 410 days after surgery. Photographs of the posterior segment of the eye (vitreous and retina) were taken with a fundus camera to evaluate postoperative inflammation of the eyes. Retinal microstructural images were obtained using spectral-domain optical coherence tomography (Cirrus high-definition OCT; Carl Zeiss, Dublin, California, USA). Retinal function was assessed using electroretinography (LW-102; Mayo, Aichi, Japan) 90 days after surgery for 6 eyes of Oligo-TetraPEG hydrogel-injected, 4 eyes of control and 4 eyes of conventional hydrogel-injected groups. Ocular examinations were performed by blinded ophthalmologists.

14. Histological evaluation of rabbit eyes

Rabbits were euthanized with an overdose of pentobarbital 410 days postoperatively, and the eyes were enucleated. After enucleation, eyes were fixed in 4% paraformaldehyde and

embedded in paraffin or OCT compound. H&E staining was performed on de-paraffinized sections (5-7 μm) and examined under a light microscope.

Data Availability

The data sets generated during and/or analyzed during the current study are available from the corresponding author on reasonable request.

References

1 Li, Y. L., Rodrigues, J. & Tomas, H. Injectable and biodegradable hydrogels: gelation, biodegradation and biomedical applications. *Chem Soc Rev* **41**, 2193-2221 (2012).

2 Anseth, K. S., Metters, A. T., Bryant, S. J., Martens, P. J., Elisseeff, J. H. & Bowman, C. N. In situ forming degradable networks and their application in tissue engineering and drug delivery. *J Control Release* **78**, 199-209 (2002).

3 Ranga, A., Lutolf, M.P., Hilborn H. & Ossipov, D. A, Hyaluronic acid hydrogels formed in situ by transglutaminase-catalyzed reaction. *Biomacromolecules* **17**, 1553-1560 (2016).

4 Pritchard, C. D, O'Shea T. M., Siegwart, D. J., Calo, E., Anderson, D. G., Reynolds, F. M., Thomas, J. A., Slotkin, J. R., Woodard, E. J. & Langer, R. An Infectable thiol-acrylate poly(ethylene glycol) hydrogel for sustained release of methylprednisolone sodium succinate. *Biomaterials* **32**, 587-597 (2011).

5 Kamata, H., Chung, U., Shibayama, M. & Sakai, T. Anomalous volume phase transition in a polymer gel with alternative hydrophilic-amphiphilic sequence. *Soft Matter* **8**, 6876-6879 (2012).

6 Li, X., Kondo, S., Chung, U. I. & Sakai, T. Degradation Behavior of Polymer Gels Caused by Nonspecific Cleavages of Network Strands. *Chem Mater* **26**, 5352-5357 (2014).

7 Kamata, H., Li, X., Chung, U.-i. & Sakai, T. Design of Hydrogels for Biomedical Applications. *Advanced Healthcare Materials* **4**, 2360-2374 (2015).

8 Kamata, H., Akagi, Y., Kayasuga-Kariya, Y., Chung, U. & Sakai, T. "Nonswellable" Hydrogel Without Mechanical Hysteresis. *Science* **343**, 873-875 (2014).

9 Ho, P. C., Chan, I. M., Refojo, M. F. & Tolentino, F. I. The Mai Hydrophilic Implant for Scleral Buckling - a Review. *Ophthalmic Surg Las* **15**, 511-515 (1984).

10 Tolentino, F. I., Roldan, M., Nassif, J. & Refojo, M. F. Hydrogel Implant for Scleral Buckling - Long-Term Observations. *Retina-J Ret Vit Dis* **5**, 38-41 (1985).

11 Marin, J. F., Tolentino, F. I., Refojo, M. F. & Schepens, C. L. Long-Term Complications of the Mai Hydrogel Intrascleral Buckling Implant. *Arch Ophthalmol-Chic* **110**, 86-88 (1992).

12 Roldan-Pallares, M., Hernandez-Montero, J., Llanes, F., Fernandez-Rubio, J. E. & Ortega, F. MIRAgel - Hydrolytic degradation and long-term observations. *Arch Ophthalmol-Chic* **125**, 511-514 (2007).

13 Flory, P. J. & Rehner, J. Statistical mechanics of cross-linked polymer networks II Swelling. *J Chem Phys* **11**, 521-526 (1943).

14 Gennes, P.-G. d. *Scaling concepts in polymer physics* (Cornell University Press,1979).

15 Sakai, T. *et al*. Design and fabrication of a high-strength hydrogel with ideally homogeneous network structure from tetrahedron-like macromonomers. *Macromolecules* **41**, 5379-5384 (2008).

16 Sakai, T. Experimental verification of homogeneity in polymer gels. *Polym J* **46**, 517-523 (2014).

17 Mours, M. & Winter, H. H. Relaxation patterns of nearly critical gels. *Macromolecules* **29**, 7221-7229 (1996).

18 Winter, H. H. & Mours, M. Rheology of polymers near liquid-solid transitions. *Adv Polym Sci* **134**, 165-234 (1997).

19 Zheng, Y. C., Li, S. P., Weng, Z. L. & Gao, C. Hyperbranched polymers: advances from synthesis to applications. *Chem Soc Rev* **44**, 4091-4130 (2015).

20 Kainthan, R. K., Muliawan, E. B., Hatzikiriakos, S. G. & Brooks, D. E. Synthesis, characterization, and viscoelastic properties of high molecular weight hyperbranched polyglycerols. *Macromolecules* **39**, 7708-7717 (2006).

21 Sakai, T., Katashima, T., Matsushita, T. & Chung, U. Sol-gel transition behavior near critical concentration and connectivity, *Polymer Journal* **48**, 629-634 (2016).

22 Wang, Q. *et al*. High-water-content mouldable hydrogels by mixing clay and a dendritic molecular binder. *Nature* **463**, 339-343 (2010).

23 Denlinger, J. L. & Balazs, E. A. Replacement of the Liquid Vitreous with Sodium Hyaluronate in Monkeys .1. Short-Term Evaluation. *Exp Eye Res* **31**, 81-99 (1980).

24 Swindle-Reilly, K. E. *et al*. Rabbit Study of an In Situ Forming Hydrogel Vitreous Substitute. *Invest Ophth Vis Sci* **50**, 4840-4846 (2009).

25 Pritchard, C. D. *et al*. Evaluation of viscoelastic poly(ethylene glycol) sols as vitreous substitutes in an experimental vitrectomy model in rabbits. *Acta Biomater* **7**, 936-943 (2011).

26 Tao, Y. *et al*. Evaluation of an in situ chemically crosslinked hydrogel as a long-term vitreous substitute material. *Acta Biomater* **9**, 5022-5030 (2013).

27 Crafoord, S., Andreasson, S. & Ghosh, F. Experimental vitreous tamponade using polyalkylimide hydrogel. *Graef Arch Clin Exp* **249**, 1167-1174 (2011).

28 Hoshi, S. *et al*. In Vivo and In Vitro Feasibility Studies of Intraocular Use of Polyethylene Glycol-Based Synthetic Sealant to Close Retinal Breaks in Porcine and Rabbit Eyes. *Invest Ophthalmol Vis Sci* **56**, 4705-4711 (2015).

29 Vink, H. Precision measurements of osmotic pressure in concentrated polymer solutions. *European Polymer Journal* **7**, 1411-1419 (1971).

30 Horkay, F., Tasaki, I. & Basser, P. J. Osmotic swelling of polyacrylate hydrogels in physiological salt solutions. *Biomacromolecules* **1**, 84-91 (2000).

Supplementary Information is linked to the online version of the paper at www.nature.com/nature.

576 **Figure Legends**

577

578 **Figure 1.** (a) Schematic illustration of gelation processes of conventional TetraPEG hydrogel
579 and Oligo-TetraPEG hydrogel. In the conventional TetraPEG hydrogel system, mutually
580 reactive TetraPEGs are simply mixed and reacted with each other to form the hydrogel. In the
581 case of the Oligo-TetraPEG hydrogel system, first mutually reactive TetraPEGs were mixed in
582 TetraPEG-SH excess and TetraPEG-MA excess conditions to form highly branched polymeric
583 clusters instead of hydrogels (Oligo-TetraPEGs). In the second *vivo* process, mutually reactive
584 Oligo-TetraPEGs were mixed to form Oligo-TetraPEG hydrogel. (b) (c) and (d) show the
585 dynamic storage modulus, G', (circles) and loss modulus, G'', (triangles) as a function of
586 frequency, ω, below, at and above the gelation threshold. In the region below the gelation
587 threshold (b, c_0 = 60 g/L, r = 0.15), the system is in the sol state and $G' < G''$. At the gelation
588 threshold (c, c_0 = 60 g/L, $r = r_c$ = 0.16), the system transforms from a sol to a gel and shows a
589 unique power law behaviour, $G' \approx G'' \approx \omega^{\beta}$. Above the gelation threshold (d, c_0 = 60 g/L, r =
590 0.17), the system is in the gel state and $G' > G''$ in a wide range of ω. All the experiments were
591 performed in triplicate and the data were averaged for each ω. The lengths of error bars (S.D.)
592 are smaller than the size of symbols.

593

594 **Figure 2.** (a) Fabrication process for Oligo-TetraPEG hydrogel through the two step process.
595 In the first process, TetraPEG-SH and TetraPEG-MA were mixed in non-stoichiometric
596 conditions to form SH-excess and MA-excess Oligo-TetraPEGs. In the second process, these
597 Oligo-TetraPEG solutions were equally diluted and mixed in equal amount to form Oligo-
598 TetraPEG hydrogels. (b) Sol-gel phase diagram: the relationship between initial polymer
599 concentration (c_0) and mixing ratio of TetraPEG-SH to total polymer concentration (r =
600 [TetraPEG-SH]/([TetraPEG-SH] + [TetraPEG-MA])) at sol-gel transition points. The
601 conditions inside the dotted line produced gels, while the conditions outside did not. All the
602 experiments were performed in triplicate and averaged. The lengths of error bars (S.D.) are
603 smaller than the size of symbols.

604

605 **Figure 3.** (a) Gelation time (t_{gel}) of Oligo-TP hydrogels (circles) and TP hydrogels (triangles)
606 as a function of the polymer concentration (c). (b) Osmotic pressure (Π_{os}) of Oligo-TP
607 hydrogels as a function of c. (c) SANS measurements from an Oligo-TP solution and an Oligo-
608 TP hydrogel. (d) Equilibrium elastic modulus (G') of Oligo-TP hydrogels (circles) and TP
609 hydrogels (triangles) as a function of c. All the experiments except for SANS measurements

were performed in triplicate and averaged. The lengths of error bars (S.D.) are smaller than the size of symbols. The error bars on the SANS profiles show S.D following complete data processing.

Figure 4. (a) Gel specimens and surrounding tissues, representative images of H&E staining and immunostaining for CD62L (GFP) in histological sections of mice at 4 weeks after subcutaneous injection of materials. Asterisks, arrows and rectangles denote materials, epidermis and the location of views of immunostaining, respectively. Nuclei were stained with DAPI. Non-specific GFP signal was detected in muscles (red dotted lines). Scale bars in H&E staining and immunostaining indicate 5 mm and 100 μm, respectively. (b) Cell proliferation of NIH3T3 cells cultured with or without Oligo-TetraPEGs. The data (relative cell number) are expressed as the mean ± SDs from four independent experiments. No statistical difference was found between MA-excess Oligo-TP and control, SH-excess Oligo-TP and control, and MA excess and SH excess Oligo-TPs in Student t-test analysis. (c) Representative H&E staining images of histological sections in mice subcutaneously injected with MA-excess and SH-excess Oligo-TPs or PBS. Sections at 3 days and 2 weeks after the injection are shown. Scale bars, 200 μm.

Figure 5. (a) Changes in the intraocular pressure in the Oligo-TP hydrogel-injected and balanced salt solution-injected (control) groups. No significant difference in intraocular pressure was observed between Oligo-TP hydrogel-injected and control groups throughout the observation period, up to 410 days in Student t-test analysis. The data are expressed as the mean ± SDs. (b) Anterior segments of rabbit eyes in the Oligo-TP hydrogel-injected, control and TP hydrogel-injected groups on postoperative day 7. (c) Images of eyes after dissection 90 days postoperatively in the Oligo-TP hydrogel-injected, control and TP hydrogel-injected groups. (d) Electroretinography waveform of rabbit eyes in the Oligo-TP hydrogel-injected, control and TP hydrogel-injected groups on postoperative day 90. Bars: 100 μV and 25 ms. (e) Electroretinography data of a-wave and b-wave implicit time in the Oligo-TP hydrogel-injected and control groups on postoperative day 90. The data are expressed as the mean ± SDs. (f) Electroretinography data of a-wave and b-wave amplitudes in the Oligo-TP hydrogel-injected and control groups on postoperative day 90. The data are expressed as the mean ± SDs. No significant difference in implicit times and amplitudes was observed between Oligo-TP hydrogel-injected and control groups. (g) Representative images of H&E staining in histological section of rabbit eyes at 410 days postoperatively. Scale bars indicate 200 μm. No apparent inflammation or alteration of retinal microstructure was observed in both Oligo-TP

hydrogel-injected and control group.

Figure 6. Fundus photography of rabbit eyes in the Oligo-TetraPEG hydrogel-injected, retinal detachment with the Oligo-TetraPEG hydrogel-injected and control groups. Arrowhead = intentional retinal break. Arrowhead = intentional retinal break.

Author Contributions

T. S. and U. C. planned and supervised the project. K. H., F. O., S. H., T. K., D. Z., X. L., M. S., E. G. and S.O. designed and performed the experiments. T. O. contributed to discussions throughout the project.

Author Information

Reprints and permissions information are available at www.nature.com/reprints.

The authors declare no competing financial interests.

Correspondence and requests for materials should be addressed to sakai@tetrapod.t.u-tokyo.ac.jp.